Chapter 2

Acoustic Wave Propagation in a Pulsed Electro Acoustic Cell

Mohamad Abed A. LRahman Arnaout

Additional information is available at the end of the chapter

http://dx.doi.org/10.5772/55271

1. Introduction

The pulsed electro-acoustic technique [1] is presented to the Electrical Engineering community where it can find many applications, from the development of improved materials for electrical insulation to the control of electrostatic surface discharge (ESD) phenomena [2]. This phenomenon could involve serious damage to the satellite structure. In order to get a better control on the discharge it is necessary to clarify the nature, the position and the quantity of stored charges with time and to understand the dynamics of the charge transport in solid dielectrics used in space environment. Since its first implementation, the PEA method has been improved and adapted to many configurations of measurement: in 2D and 3D resolution [3] [4], with remote excitation [5] [6], on cables [7] [8] and under alternative stress [9] [10].

Recently, based on the PEA method, two original setups to measure space charge distribution in electron beam irradiated samples have been developed, and are called 'open PEA' and 'Short-Circuit PEA'. One of the weaknesses of this current technique is spatial resolution, about 10 μm. Indeed, dielectrics materials used in satellite structure have a thickness around 50 μm. Our work aims at improving the spatial resolution of a cell measurement by analyzing: electrical component, signal treatment, electrode material and sensor. In this paper, we only focused on the study of acoustic wave generation and their propagation. An electro-acoustic model has been developed with commercial software COMSOL®. This model is one-dimensional, and system of equations with partial differential functions is solved using a finite element method in non-stationary situations. Results show the propagation of acoustic wave vs. time in each part of cell measurement: sample, electrodes, piezoelectric sensor, and absorber. Influence of sensor geometry on the quality of output signal is also analyzed.

2. PEA method

The PEA measurement principle is given in Figure 1. Let us consider a sample having a thickness d presenting a layer of negative charge ρ at a depth x. This layer induces on the electrodes the charges ρ_d and ρ_0 by total influence so that:

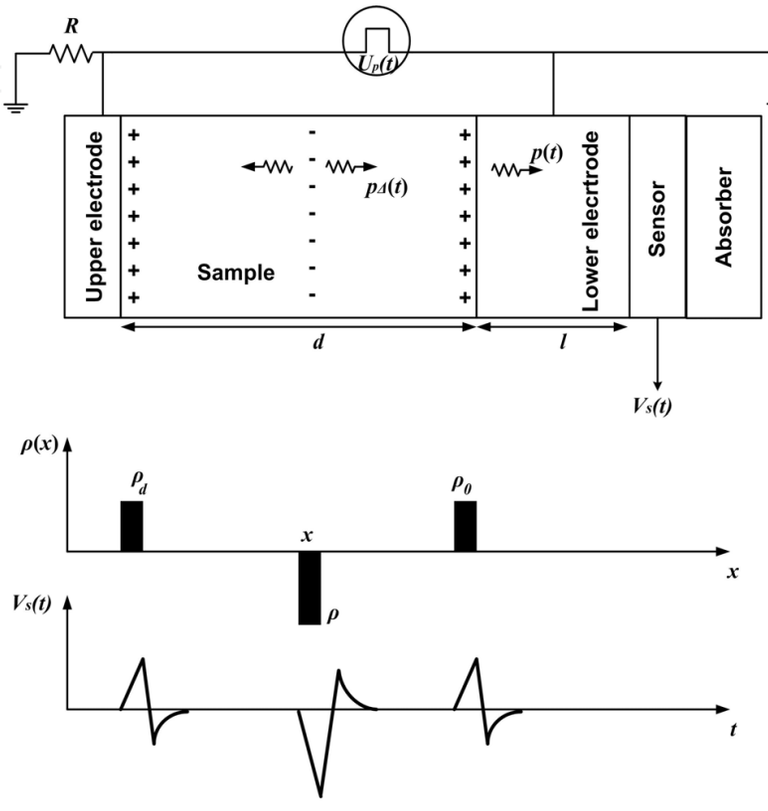

Figure 1. Schematic diagram of a PEA system.

$$\rho_d = \frac{-x}{d}\rho$$
$$\rho_0 = \frac{x-d}{d}\rho \tag{1}$$

Application of a pulsed voltage $U_p(t)$ induces a transient displacement of the space charges around their positions along the x-axis under Coulomb effect. Thus elementary pressure waves $p_\Delta(t)$, issued from each charged zone, with amplitude proportional to the local charge density propagates inside the sample with the speed of sound. Under the influence of these pressure variations, the piezoelectric sensor delivers a voltage $V_s(t)$ which is characteristic of the pressures encountered. The charge distribution inside the sample becomes accessible by acoustic signal treatment.

The expression of pressure waves reaches the piezoelectric detector is as follows:

$$p(t) = \int_{-\infty}^{+\infty} p_\Delta(x,t) = \int_{-\infty}^{+\infty} U_p\left(t - \frac{l}{v_e} - \frac{x}{v_s}\right).\rho(x).dx \tag{2}$$

With, v_e and v_s are the sound velocity of the electrode and the sample respectively.

Various parameters relevant to the spatial resolution of PEA method are clearly identified: as the thickness of the piezoelectric sensor, the bandwidth of system acquisition, etc... To quantify the influence of each parameter, a simplified electro acoustic model is proposed based on PEA cell.

3. Simulation set up

Our approach consists to establish an electro acoustic model from five sub-domains which represent the essential PEA cell element [11]. Each sub-domain is defined by the material and the thickness Table 1. As the samples are very thin compared to the lateral dimensions, we will consider a one-dimensional modelling. Each element is defined by a segment of length equal to the actually thickness.

Sub-domain	Material	Thickness (μm)
Upper electrode	**Linear Low Density Poly Ethylene (LLDPE)**	**1000**
Sample	**Poly Tetra Fluoro Ethylene(PTFE)**	**300**
Lower electrode	**Aluminum**	**10 000**
Piezoelectric sensor	**PolyVinyliDene Fluoride(PVDF)**	**1→9**
Absorber	**Poly Methyl Meth Acrylate (PMMA)**	**2000**

Table 1. Characteristics of each sub-domain in PEA model

Theoretically, the acoustic wave propagation is completely described by a partial differential equation (3).

$$\frac{1}{\rho_0 c^2}\frac{\partial^2 p}{\partial t^2}+\frac{\partial}{\partial x}(-\frac{1}{\rho_0}(\frac{\partial p}{\partial x}-q))=Q_{\text{int}} \tag{3}$$

Where p represents the acoustic pressure ($N.m^{-2}$), c sound velocity ($m.s^{-1}$), ρ_0 density of material ($kg.m^{-3}$), q ($N.m^{-3}$) and Q_{int} ($N.kg^{-1}.m^{-1}$) reflect respectively the effect of external and the internal forces in the domain.

Acoustic pressure is obtained by resolving equation 3. In order to simplify our model, some assumptions are defined below:

- Attenuation and dispersion are not taken into account.
- Acoustic waves are generated by Coulomb forces created by the application of electric pulse on the electric charges present in sample.
- There is no acoustic source within the model: $Q_{int} = 0$.

After these assumptions (3) becomes:

$$\frac{1}{\rho_0 c^2}\frac{\partial^2 p}{\partial t^2}+\frac{\partial}{\partial x}(-\frac{1}{\rho_0}(\frac{\partial p}{\partial x}-q))=0 \tag{4}$$

Given the different assumptions, we have grouped the five sub-domains into three categories.

- Sub-domain which contains an acoustic source: sample, upper and lower electrode.
- Sub-domain that excludes acoustic source: absorber (PMMA).
- Piezoelectric sub-domain: piezoelectric sensor (PVDF).

Acoustic wave behavior in PEA simplified model depends on the acoustic impedance of each sub-domain. This impedance is equal to the product of sound velocity and density of material Table 2.

Sub-domain	**Upper electrode**	**Lower electrode**	**Sample**	**Piezoelectric sensor**	**Absorber**
ρ_0 (kg.m^{-3})	**940**	**2700**	**2200**	**1780**	**1190**
c (m.s^{-1})	**2200**	**6400**	**1300**	**1270**	**2750**
Z ($kg.m^{-2}.s^{-1}$)	**2068 x10^3**	**17280 x10^3**	**286 x10^3**	**2260.6 x10^3**	**3272.5 x10^3**

Table 2. Acoustic parameters of each sub-domain in the model.

The application of an electric field on a sample (which contains electric charges) induces a mechanical force. This force consists of four terms [12] (5).

$$q_k=-\frac{1}{2}E_i.E_j\frac{\partial \varepsilon_{ij}}{\delta x_k}-\frac{1}{2}.\frac{\partial(\alpha_{ijkl}\cdot E_i\cdot E_j)}{\delta x_l}+\rho.E_k+kp_i.\frac{\partial E_k}{\partial x_i} \tag{5}$$

With:

- $\frac{1}{2}E_i.E_j\frac{\partial \varepsilon_{ij}}{\delta x_k}$: force produced by the variation of the electric permittivity.
- $\frac{1}{2}.\frac{\partial(\alpha_{ijkl}\cdot E_i\cdot E_j)}{\delta x_l}$: force provided by electrostriction effect.
- $\rho.E_k$: force created by the presence of electric charge in the sample.
- $kp_i.\frac{\partial E_k}{\partial x_i}$: force produced by the presence of electric dipoles in the sample.
- E_i, E_j, E_k: electric field components.
- ε_{ij}: electric permittivity.
- α_{ijkl}: electrostriction tensor.
- ρ: electric charge in the sample.
- kp_i: electric dipoles coefficient.

In 1D and without electric dipole equation (5) is:

$$q = -\frac{1}{2}E^2\frac{\partial \varepsilon}{\partial x} - \frac{1}{2}\frac{\partial(\alpha E^2)}{\partial x} + \rho E \tag{6}$$

Knowing that: $div(E) = \frac{\rho}{\varepsilon}$

$$q = -\frac{1}{2}E^2\frac{\partial \varepsilon}{\partial x} - \frac{1}{2}\frac{\partial(\alpha E^2)}{\partial x} + E\frac{\partial \varepsilon E}{\partial x} \tag{7}$$

Considering that: $\frac{\partial \varepsilon E^2}{\partial x} = \varepsilon E\frac{\partial E}{\partial x} + E\frac{\partial \varepsilon E}{\partial x}$ so

$$q = -\frac{1}{2}E^2\frac{\partial \varepsilon}{\partial x} - \frac{1}{2}\frac{\partial(\alpha E^2)}{\partial x} + \frac{\partial \varepsilon E^2}{\partial x} - \varepsilon E\frac{\partial E}{\partial x} = -\frac{1}{2}E^2\frac{\partial \varepsilon}{\partial x} - \frac{1}{2}\frac{\partial(\alpha E^2)}{\partial x} + \frac{\partial \varepsilon E^2}{\partial x} - \frac{1}{2}\varepsilon\frac{\partial E^2}{\partial x} \tag{8}$$

Recognizing that: $-\frac{1}{2}E^2\frac{\partial \varepsilon}{\partial x} - \frac{1}{2}\varepsilon\frac{\partial E^2}{\partial x} = -\frac{1}{2}\frac{\partial \varepsilon E^2}{\partial x}$ therefore,

$$q = -\frac{1}{2}\frac{\partial \varepsilon E^2}{\partial x} - \frac{1}{2}\frac{\partial(\alpha E^2)}{\partial x} = \frac{1}{2}\frac{\partial((\varepsilon - \alpha)E^2)}{\partial x} \tag{9}$$

Due to the application of electric pulse, the electric field varies from E to $E+\Delta E(t)$, so (9) becomes:

$$q = \frac{1}{2}\frac{\partial((\varepsilon - \alpha)E^2)}{\partial x} + \frac{\partial((\varepsilon - \alpha)(E\Delta E(t))}{\partial x} + \frac{1}{2}\frac{\partial((\varepsilon - \alpha)(\Delta E(t)^2)}{\partial x} \tag{10}$$

In order to simplify our model we consider that α=0 and ΔE, ε are uniforms. After simplification of (10), the mechanical force in our model is the product of electric charges present in sample by the applied electric pulse.

$$q = \rho.\Delta E(t) \tag{11}$$

In our model we consider that:

- Electric charge profile ϱ is established by three Gaussian shapes of width = 3μm. A normalized negative one at sample center and two positives at sample interfaces Figure 2-a.
- A normalized square electric pulse which has a 5ns pulse width that has almost the same value of the experimental pulse Figure 2-b.

Piezoelectric transducer is used to convert electrical energy into mechanical energy and vice versa. The active element is basically a piece of polarized material, PVDF in our case. When the acoustic wave propagates in the PVDF, an electric voltage will appear at its interface, which it related to the direct piezoelectric effect [13].

The piezoelectric relations are given in equation (12).

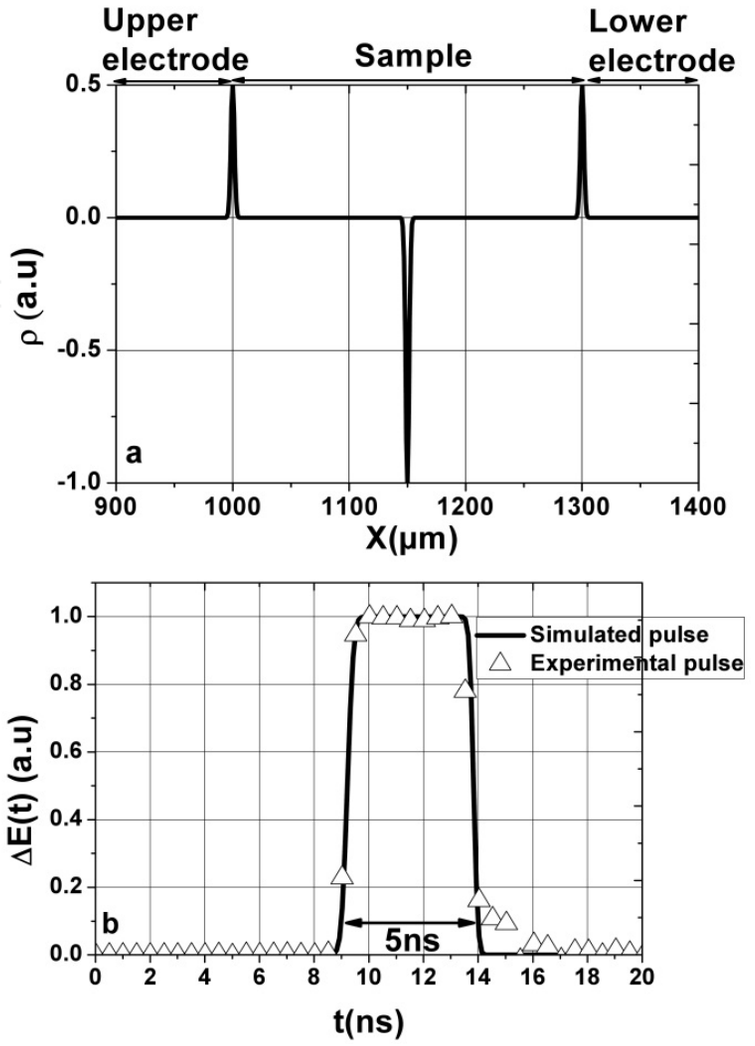

Figure 2. Modeling of mechanical force which is the product of electric charge distribution represented in (a) and the electric pulse represented in (b).

$$\begin{cases} D_i = d_{ikl} T_{kl} + \varepsilon_{ij}^{T} E_j \\ S_{ij} = s_{ijkl}^{E} T_{kl} + d_{ijk} E_k \end{cases} \tag{12}$$

With, D_i is the electric charge density displacement, E_i the electric field, S_{ij} the strain and T_{kl} the stress. s^{E}_{ijkl} is the compliance, ε^{T}_{ij} the permittivity. d_{ikl} is the matrix for the direct piezoelectric effect and d_{ijk} is the matrix for the converse piezoelectric effect.

In one dimension and referring to PEA case (D=0 because we have an open circuit configuration and T_{kl}=-p), the electric field vs. pressure waves is written as follow:

$$E_{PVDF} = \frac{d_{33}}{\varepsilon_{33}^{T}} p = g_{33} p \tag{13}$$

Output voltage signal can be obtained by integrating the electric field i.e. pressure wave along the PVDF thickness:

$$V = -\int_0^{d_{PVDF}} E_{PVDF}(x)dx = \int_0^{d_{PVDF}} -g_{33}p(x)dx \tag{14}$$

3.1. Sub-domain without acoustic source

This case represents the PMMA absorber. In principle, this material (PMMA) is used to avoid reflections of waves at the interface with the piezoelectric sensor. Unfortunately due to the difference between their acoustic impedance, we always have acoustic wave reflection at its interfaces. We estimate acoustic pressure in this sub-domain by neglecting the acoustic source, q = 0 in (4).

3.2. Boundary conditions

In our model, two kinds of boundary conditions are considered:

- *Dirichlet boundary condition*: pressure at external interfaces is considered as null in our model (upper electrode and PMMA):

$$p = 0 \tag{15}$$

- *Continuity condition*: The internal interfaces of the geometry are specified by the continuity of velocity vibration and acoustic pressure:

$$\frac{1}{\rho_i} \times \left(\nabla p_i - q_i\right) = \frac{1}{\rho_{i+1}} \times \left(\nabla p_{i+1} - q_{i+1}\right) \tag{16}$$

4. Simulation results

Simulation of acoustic wave in the model is realized by the commercial software Comsol. This software is based on the finite element method [14]. The domain of calculation is divided into several uniform elements of width Δx. Time step, Δt, in the computation is chosen with respect to Friedrich-Levy [15] condition:

$$\Delta t < \frac{\Delta x}{c} \tag{17}$$

In our model Δx = 1μm and Δt = 0.1 ns.

Figure 3 shows the pressure for T=20 ns, for 300μm sample thick and 9μm sensor thick. This figure is divided into three regions. The sample is presented in region 2, however regions 1 and 3 represent respectively, and the adjacent upper and lower electrode. An electrical pulse is applied to probe the space charge distribution. Under the effect of the electric field pulse, the charges are shifted and come back to their original position, creating an acoustic wave (Coulomb forces effect).

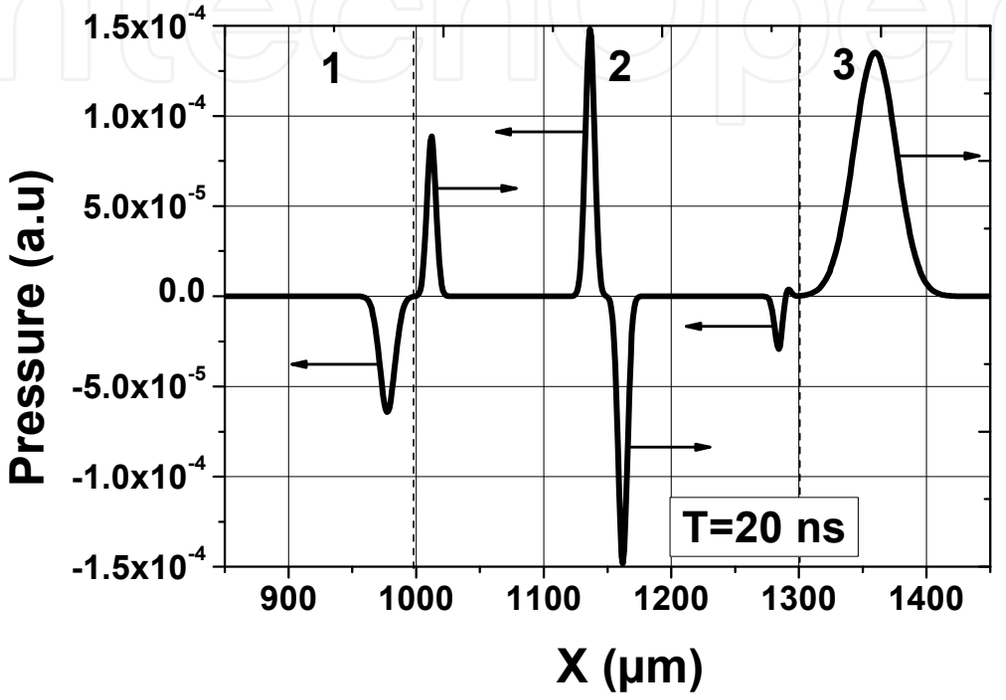

Figure 3. Acoustic wave generation in the sample.

When acoustic wave is completely generated for T=20 ns, we observe two pressure waves move at opposite way Figure 3: the first (at the left of Figure 3) moves towards the upper electrode and the second (at the right of Figure 3) moves towards the lower electrode. We can also observe a spreading more important for the pressure wave inside the lower electrode than the wave inside sample. This feature goes with the different values of the sound velocity between PTFE (sample) and Aluminum (lower electrode) Table 2. The same conclusion can be done for the upper electrode; value of sound velocity for the upper electrode is about 2 times larger than the sample.

Figure 4 shows acoustic wave for T=0 across the five sub-domains of PEA model i.e. upper electrode, sample, lower electrode, piezoelectric sensor and the absorber.

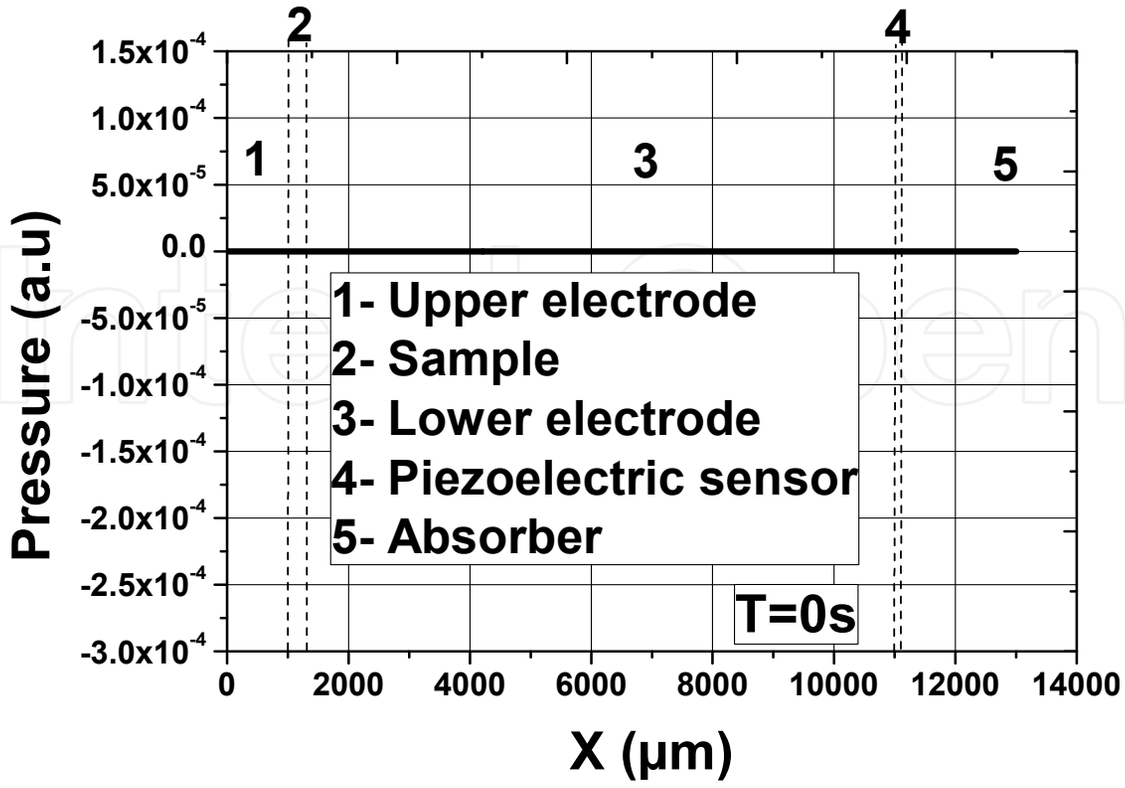

Figure 4. PEA model for T=0s.

For t= 800 ns we observe that the useful signal moves through lower electrode, Figure 5-a, and reaches the piezoelectric transducer at $t = 1.5$ μs, Figure 5-b. These results show that reflexion phenomena induce a lot of unwanted signals able to disturb the quality of the useful signal.

Figure 6 shows the output voltage signal for the five values of sensor thickness.

Only the useful signal (that its shape corresponds to the charge shape) has been integrated along the PVDF thickness referred to equation (14). We can observe when the sensor thickness decreases and reaches 1 μm, the output voltage signal leads to the same shape of space charge distribution inside the sample, Figure 2-a. For a larger thickness than 1 μm, the shape leads to a very different shape of the space charge distribution. The reflexion of acoustic waves on PVDF and PMMA interfaces plays an essential role in this case and involves some interference between the incident wave and reflected wave. This interference leads to a degradation of the output signal as shown in Figure 8. In order to improve the quality of this signal for thicknesses larger than 1 μm, it will be necessary to adapt acoustic impedances between sensor and absorber.

PMMA absorber is a related component with the piezoelectric sensor. Due to the difference between the acoustic impedance of these both materials, the transmission of acoustic waves is not optimally performed. Only a part of the wave is transmitted to the absorber, the other part is reflected on the interface and interferes with the incident wave. To improve the transmission coefficient wave, an acoustic impedance matching must be done i.e. the related materials should have the same acoustic impedance which is the product of material density

and material sound velocity. Therefore, in our study, the PMMA absorber is replaced by a PVDF.

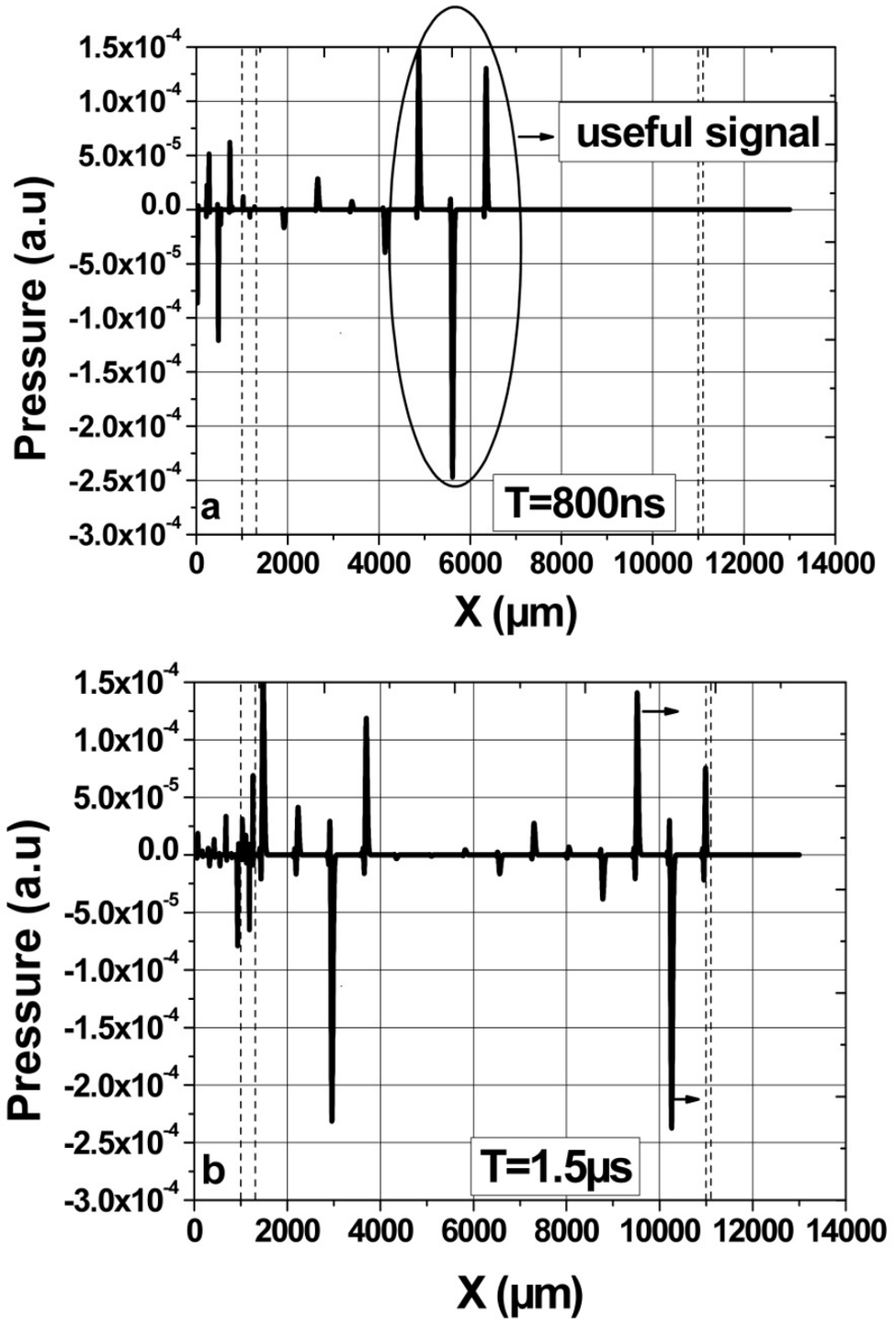

This simulation has been realized with a piezoelectric transducer thickness equal to 9 µm. With different sensors thicknesses, the same pressure wave evolution has been observed between sample and sensor (sensor not included). Only the shape of the output voltage signal is affected by the transducer thickness.

Figure 5. Acoustic wave propagation in the model . a) for T=800ns.b) for T=1.5µs

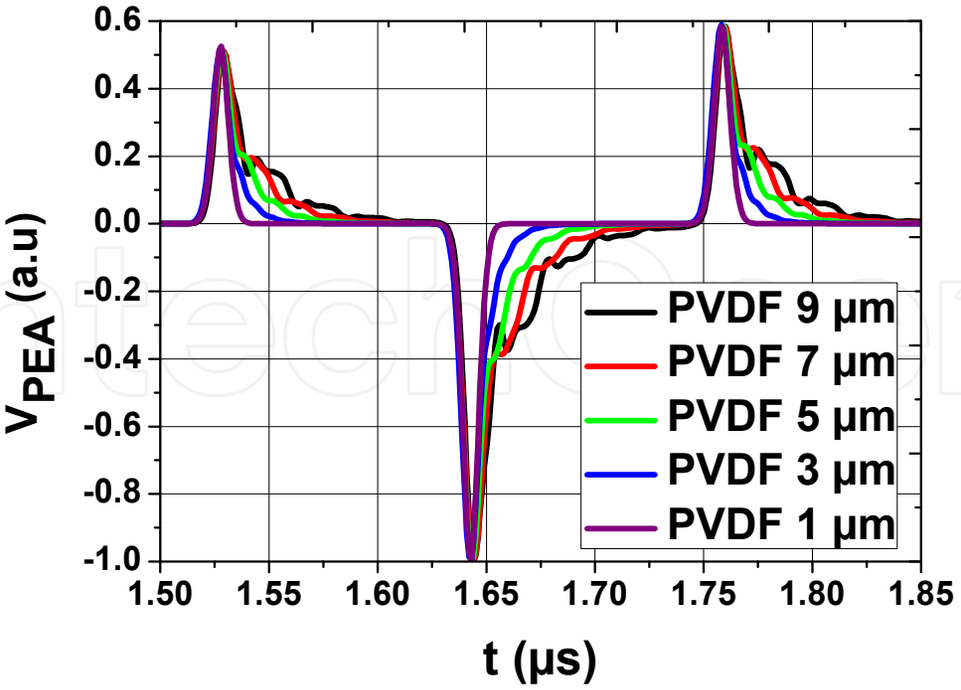

Figure 6. Potential signal for different PVDF thicknesses

Figure 7 shows the output voltage of piezoelectric sensor with and without a matched interface. The thickness of the sensor is fixed at 9 µm. This figure shows clearly the influence of the acoustic impedance on the quality of the output signal. Indeed, the reflected wave at the interface of PVDF / PMMA induces a strong distortion of the voltage signal that appears at each part of the useful signal. This distortion may affect the data processing, so a matched interface must be realized during the design of the new optimized cell.

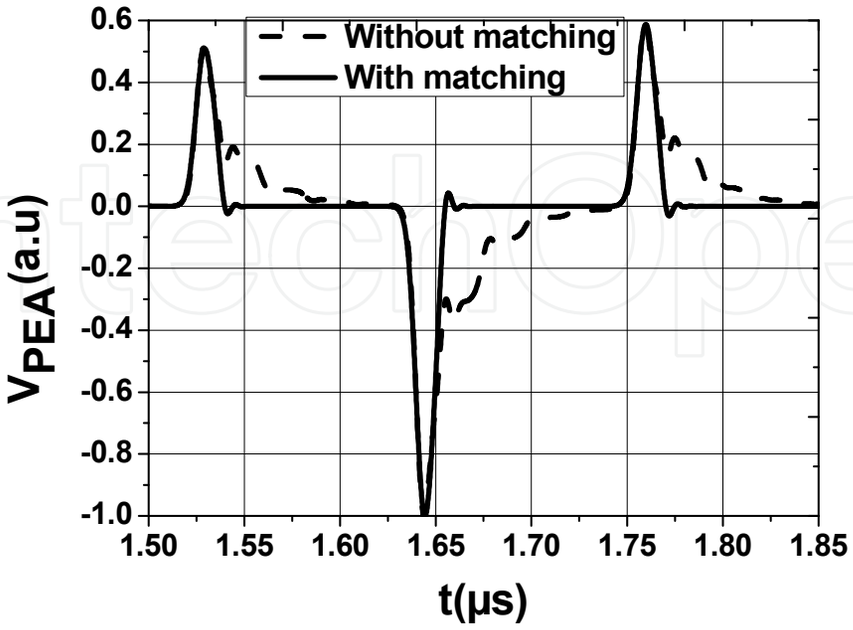

Figure 7. PVDF output signal with and without a matched interface between the sensor and the absorber

5. Analysis

Figure 7 shows a block diagram of a simplified PEA cell. In our case, voltage amplifier is considered ideal with a gain equal to 1 (infinite bandwidth). In this block diagram, input data is the distribution of net density of charge in the sample (charges at the both electrodes and in the bulk), denoted ϱ, and the output data is the piezoelectric sensor voltage, denoted V_{PEA}.

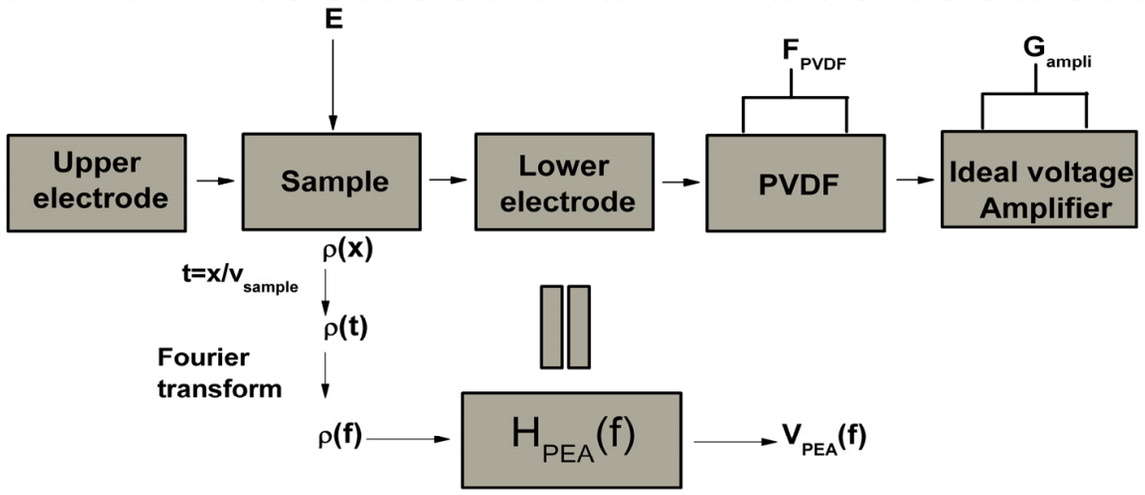

Figure 8. PEA bloc diagram

According to this figure, equations (18) and (19), written in frequency domain, will allow defining the transfer function matrix:

$$H_{PEA}(f) = E(f) \times F_{PVDF}(f) \times G_{ampli}(f) \tag{18}$$

$$V_{PEA}(f) = H_{PEA}(f)\rho(f) \tag{19}$$

Where F_{PVDF} and G_{ampli} are the transfer function respectively of PVDF sensor and voltage amplifier. According to (19) output voltage, is defined as a convolution product between transfer function and net density of charge in the studied dielectric:

$$v_{PEA_i} = \sum h_{PEA\,i,j}\rho_j \tag{20}$$

Convolution being the sum of the product of one function with the time reversed copy of the other function, a symmetric Toeplitz matrix can be used to define H_{PEA} [16]. This diagonal-constant matrix is a matrix in which each descending diagonal from left to right is constant. It is especially used for discrete convolution and it is completely determined by the first row. The following matrix A illustrates a symmetric Toeplitz matrix of order n and the following vector v represents exactly the same matrix A shown above where:

$$A_{ij} = a_{i-1,j-1} \text{ for i = 2, n and j = 2, n}$$

$$A = \begin{pmatrix} a_{11} & a_{21} & . & a_{n1} \\ a_{21} & a_{11} & . & . \\ . & . & . & a_{21} \\ a_{n1} & . & a_{21} & a_{11} \end{pmatrix} \quad v = \begin{pmatrix} a_{11} \\ a_{21} \\ . \\ a_{n1} \end{pmatrix} \tag{21}$$

In our case, vector v is the impulse response i.e. the values of the first peak of output voltage for a polarized material, (denoted and usually named "calibration signal") and hence, equation (19) can be re-written as a linear function:

$$\underbrace{\begin{pmatrix} v_{PEA1} \\ v_{PEA2} \\ . \\ v_{PEAn} \end{pmatrix}}_{V_{PEA}} = \underbrace{\begin{pmatrix} v_{ref1} & v_{ref2} & . & v_{refn} \\ v_{ref2} & v_{ref1} & . & . \\ . & . & . & v_{ref2} \\ v_{refn} & . & v_{ref2} & v_{ref1} \end{pmatrix}}_{H_{PEA}} \underbrace{\begin{pmatrix} \rho_1 \\ \rho_2 \\ . \\ \rho_n \end{pmatrix}}_{\rho} \tag{22}$$

Using the simulated, it is relatively easy to define the transfer function matrix. Knowing V_{PEA} and H_{PEA} the purpose of the next section is to analyze and to improve the condition number of H_{PEA} matrix.

In numerical analysis, the condition number of a matrix, denoted C in equation (23), measures the dependence of the solution compared to the data problem [17], in order to check the validity of a computed solution with respect to its data. Indeed, data from a numerical problem depends on experimental measurements and they are marred with error. We can say the condition number associated with a problem is a measure of the difficulty of numerical problem calculation. A problem with a condition number close to 1 is said to be well-conditioned problem, while a problem with a high condition number is said to be ill-conditioned problem. The condition number of the PEA Toeplitz matrix is equal to 400,000 and hence this very high value shows that our system is very ill-conditioned.

$$C = \left\| H_{PEA} \right\|_2 \left\| H_{PEA}^{-1} \right\|_2 \tag{23}$$

Where;

$$\left\| H_{PEA} \right\|_2 = \sqrt{\max(\det({H_{PEA}}^t \cdot H_{PEA} - \lambda I))}$$

λ : Eigenvalues of H_{PEA}.

i. Identity matrix

The identification method of the matrix is preserved; our goal is to improve the matrix condition number by studying the influence of intrinsic parameters for a PEA cell. Three parameters are studied: the thickness of piezoelectric sensor, the shape of pulse voltage, and the matching interfaces.

Table 3 shows condition number values for different PEA configuration. As we can see on this table, a "theorical" optimized cell measurement can be defined using a piezo-electric of 1μm, an impedance matching for all materials interfaces, and applying a Gaussian shape for electrical pulse. The condition number for this optimized cell is about 200 times smaller than the one from classical measurement cell! However, it should be noted that the choice of a Gaussian pulse decreases the expected resolution of the measure, it will be necessary to establish eventually a compromise between high spatial resolution and a well-posed system.

Thickness of PVDF	Pulse Shape	Matching interfaces	Condition number
9μm	Square	without matching	4.13 x 105
1μm	Square	without matching	4.2 x 104
9μm	Gaussian	without matching	9.2 x 104
9μm	Square	(PVDF/PMMA)	5.4 x 104
9μm	Square	(Electrode/sample)	1.3 x 105
1um	Gaussian	All interfaces	2 x 103

Table 3. Impact of PEA intrinsic parameters on transfer matrix condition number

In the next section, different deconvolution techniques are going to be used in order to recover the repartition of the net density of charge imposed on the Comsol model.

Wiener filtering is commonly used to restore degraded signals or images by minimizing mean square error. It is based on a statistical approach i.e. this filter is assumed to have knowledge of the spectral properties of the original signal and noise. Wiener filter must be physically realizable and causal and it is frequently used in the process of deconvolution. In frequency domain, its equation can be written as following:

$$H_{Wiener}(f) = \frac{1}{H_{PEA}(f)}\left[\frac{\left|H_{PEA}(f)\right|^2}{\left|H_{PEA}(f)\right|^2 + \frac{1}{SNR(f)}}\right] \tag{24}$$

and equation (19) becomes:

$$\rho(f) = H_{Wiener}(f)V_{PEA}(f) \tag{25}$$

Where ; H_{PEA} is the transfer function matrix and $SNR(f)$ the signal-to-noise ratio. When there is zero noise (i.e. infinite signal-to-noise), the term inside the brackets equals 1, which means that the Wiener filter is simply the inverse of the system. However, as the noise at certain frequencies increases, the signal-to-noise ratio drops, so the term inside the square bracket also drops. This means that the Wiener filter attenuates frequencies dependent on their signal-to-noise ratio. As explain previously, the condition number for H_{PEA} is relatively high and the coefficient $a = 1/SNR(f)$ will be estimated using L-Curve method.

The L-Curve method consists of the analysis of the piecewise linear curve whose break-point are:

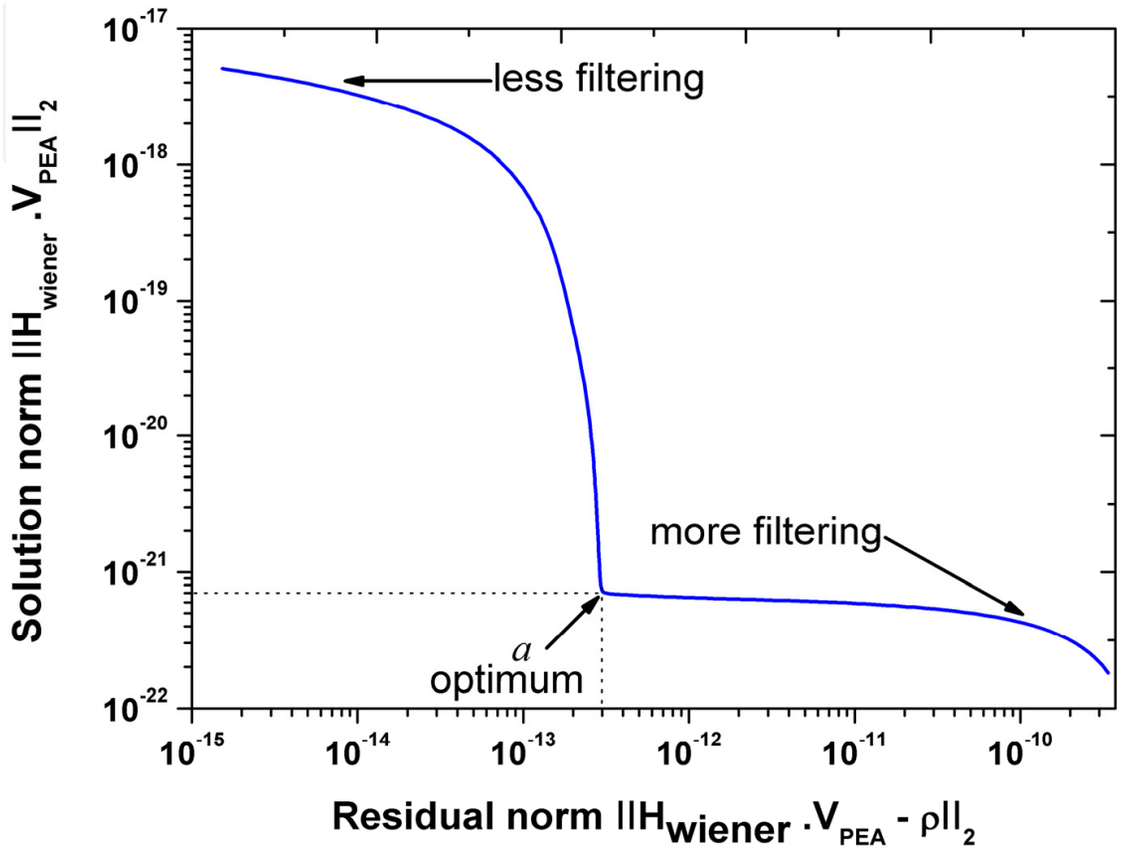

Figure 9. L-curve shape for unoptimized PEA cell

This curve, in most cases, exhibits a typical "L" shape, and the optimal value of the regularization parameter a is considered to be the one corresponding to the corner of the "L", Figure 10 [18-19]. The corner represents a compromise between the minimization of the norm of the residual and the semi-norm of the solution. This is particular evident in Fig.8, the horizontal branch of the "L" is dominated by the regularization error, while the vertical branch shows the sharp increase in the semi-norm caused by propagation errors.

Our approach consists to establish the deconvolved charge by using the transfer matrix H_{PEA} which was established. Gaussian filter is not accounted. The main objective of this section is to analyze the shape of the recovered charges using current PEA cell and the shape of the recovered charges using an optimized cell.

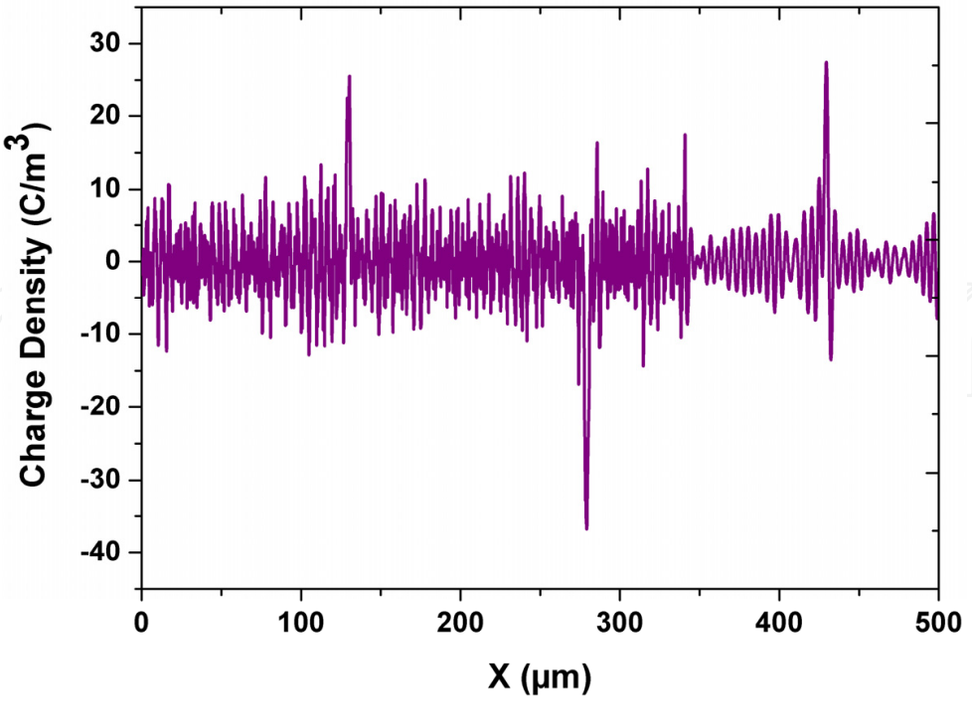

Figure 10. Net density of charges estimated using Wiener filter and a =8x10-21 Current PEA cell with C = 400,000 for H_{PEA}

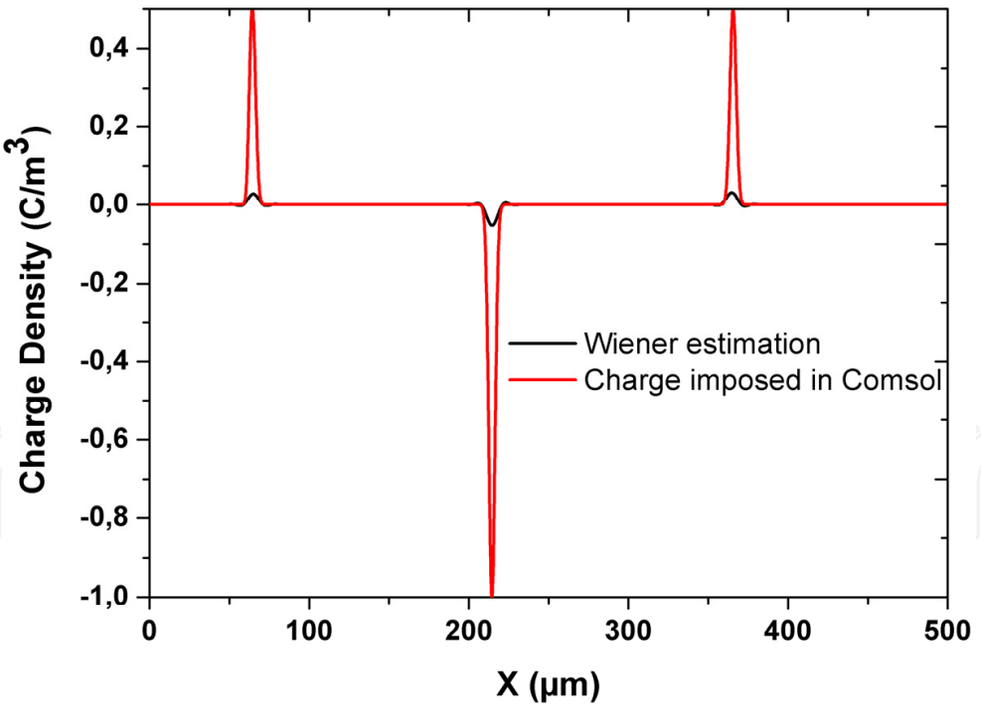

Figure 11. Net density of charges estimated using Wiener filter and a =3x10-12 Optimized PEA cell with C = 2,000 for H_{PEA}

Results presented in Figure 10 and Figure 11 show the net density of charges estimated by Wiener method using the current PEA cell, Figure 10, and using an optimized cell, Figure 11.

Figure 10 shows that the recuperated charges by Wiener deconvolution are completely wrong, only noise is recovered and amplified! The inversion of this matrix is equivalent to applying a high pass filter, thus amplifying any high frequency noise. That is mainly for this reason that a Gaussian filter is usually applied for the signal treatment of PEA cell.

Using an optimized cell, result shown in Figure 11 has the similar shape, but unfortunately its amplitude is lower by 10 times than the net density of electric charge, and presents oscillations on both sides of the useful signal. These observations are typical of the adjustment when the system is ill conditioned. It is a compromise between filtering, and precision. This compromise is achieved by the settlement of regularized parameters determined by L-Curve method. Based on the previous results, the further work aims to redefine the method used for the calibration signal in order to have a condition number much more less than one obtained previously.

6. Conclusion

A one-dimensional numerical model based on acoustic wave propagation and established using COMSOL® was developed for a PEA cell with the objective to understand how sensor thickness is involved in the output voltage signal. In this model, transmission and reflection are taken into account, only attenuation and diffusion are neglected. Partial differential equation has been resolved using finite element method. In this paper, simulation results have been presented for different thicknesses of PVDF sensor from 1 μm to 9 μm. Results show the interest to use an ultra-thin piezoelectric sensor for improving the spatial resolution of the PEA cell. This model also permits to analyze acoustic wave behavior from its generation in sample to its conversion to an electric signal by piezoelectric transducer. Referred to this model, a PEA transfer function has been developed using a Toeplitz matrix, kind of matrix based on convolution principle. In order to improve the condition number of the transfer matrix, an optimized PEA cell has been defined based on a piezo-electric of 1μm, an impedance matching for all materials interfaces, and applying a Gaussian shape for electrical pulse. Deconvolution results show that a high condition number involves a strong deformation of estimated charge compare to a condition number much lower. Moreover, this study has highlighted the limits of regularization when the matrices are ill-conditioned: presence of oscillations, loss of information, etc.

Author details

Mohamad Abed A. LRahman Arnaout
Toulouse University, Plasma and Energy Conversion Laboratory, Toulouse, France

7. References

[1] Takada T Maeno T and Kushibe H (1987) An electric stress-pulse technique for the measurement of charges in plastic plate irradiated by an electron beam IEEE Trans. Electr. Insul. 4 pp 497-501.

[2] Blaiman Keith G (1996) Space experiment design for electrostatic charging and discharging Proc. Int Conference on Astronautics pp115-122.
[3] Maeno T (2001) Three-dimensional PEA Charge Measurement System IEEE Trans. Dielectr. Electr. Insul. 8 pp 845-848.
[4] Fukuma M Maeno T and Fukunaga K (2005) High Repetition Rate Two-dimensional Space Charge Measurement System Proc. Int Symposium on Electrical Insulating Materials -Kitakyushu pp 584-587.
[5] Griseri V Fukunaga K Maeno T Laurent C Levy L and Payan D (2004) Pulsed Electro-acoustic Technique Applied to In-situ Measurement of Charge Distribution in Electron irradiated Polymer IEEE Trans. Dielectr. Electr. Insul.11 pp 891-898.
[6] Perrin C (2007) Apport de la technique électro-acoustique pulsée à la mesure et à l'analyse du transport de charges dans les diélectriques sous faisceau d'électron (Toulouse III University) pp 1-162.
[7] Bodega R 2006 Space Charge Accumulation in Polymeric High Voltage DC Cable Systems -Delft University pp 1-183.
[8] Muronaka T Tanaka Y Takada T Maruyama S and Mutou H (1996) Measurement of Space Charge Distribution in XLPE Cable using PEA system with Flat Electrode Annual Report Conference on Electrical Insulation and Dielectric Phenomena pp 266-269.
[9] Alison JM Dissado LA and Fothergill JC (1998) The pulsed-electro-acoustic method for the measurement of the dynamic space charge profile within insulators The dielectrics society pp 93-121.
[10] Thomas C Teyssedre G and Laurent C(2008) A New Method for Space Charge Measurements under Periodic Stress of Arbitrary Waveform by the Pulsed Electro-acoustic Method IEEE Trans. Dielectr Electr Insul. 15 pp 554-559.
[11] Bernstein J.B (1991) Analysis of the electrically stimulated acoustic wave method for observing space charge in semi-insulating films Phvs. Rev. *B*. 44 pp 10804-10814.
[12] Holé S and Ditchi T (2000) Influence of divergent electric fields on space-charge distribution measurements by elastic methods Phys. Rev. *B*. 61. pp.13528-13539
[13] Berquez. L and Franceschi J.L (1998) Modeling and characterization of transducers for therrnoacoustic signal Sensors and Actuators A: Physical , pp. 115-120.
[14] Cook R.D Malkus D.S and Plesha M.E (1989) Concepts and Applications of Finite Element Analysis, 3rd Ed., JohnWiley and Sons.
[15] Kesserwani G Ghostine R Vazquez J Mosé R and Ghenaim A (2007) Simulation unidimensionnelle de l'écoulement à surface libre avec un schéma numérique TVD en discrétisation implicite et explicite La Houille Blanche 5 pp 101-106.
[16] Gray R.M, Toeplitz and circulant Matrices (2006) AReview Foundations and Trends® in communications and Information theory 2 pp155-239,.
[17] Tikhonov A.N Arsenin V.Y (1997) Solution of ill-posed problems wiley New York.
[18] Hansen P.C 1994 Regularization Tools: A MATLAB package for analysis and solution of discrete ill-posed problems Num. Algoritms 6 pp1-35.
[19] Hansen P.C O'Leary D.P (1993) The use of the L-Curve in the regularization of discrete ill-posed problems SIAMJ.Comput 14 N.6 pp 1487-1503.